Regional, seasonal, and inter-annual variations of Antarctic and sub-Antarctic temperature anomalies related to the Mansurov effect

Environmental Research Communications

LETTER

Regional, seasonal, and inter-annual variations of Antarctic and sub-Antarctic temperature anomalies related to the Mansurov effect

Mervyn P Freeman[1] **and Mai Mai Lam**[2]

[1] British Antarctic Survey, Cambridge, United Kingdom
[2] Department of Meteorology, University of Reading, Reading, United Kingdom

E-mail: mpf@bas.ac.uk

Keywords: Mansurov effect, surface temperature, Antarctic, global atmospheric electric circuit

OPEN ACCESS

RECEIVED
27 March 2019

REVISED
15 August 2019

ACCEPTED FOR PUBLICATION
3 October 2019

PUBLISHED
29 October 2019

Abstract

We use National Centers for Environmental Prediction/National Center for Atmospheric Research reanalysis data to show that Antarctic surface air temperature anomalies result from differences in the daily-mean duskward component, B_y, of the interplanetary magnetic field (IMF). We find the statistically-significant anomalies have strong geographical, seasonal, and inter-annual variations. For the interval 1999–2002, regional anomalies poleward of 60°S are of diminishing representative peak amplitude from autumn (3.2 °C) to winter (2.4 °C) to spring (1.6 °C) to summer (0.9 °C). Exploiting apparently simplifying properties in the sub-Antarctic region in autumn 1999–2002, we demonstrate that temperature anomalies in this case are due to geostrophic wind anomalies, resulting from the same B_y changes, moving air across large meridional gradients in zonal mean air temperature between 50 and 70°S over the 7-hour timescale for which a change in B_y can be expected to persist. Since the tropospheric pressure anomalies causing these winds have been associated with B_y-driven anomalies in the electric potential of the ionosphere, we conclude that IMF-induced changes to the global atmospheric electric circuit can cause day-to-day changes in regional surface air temperature of up to several degrees Centigrade.

1. Introduction

The effects of solar variability are still major unknowns in our understanding of weather and climate, and hence inadequately represented in atmospheric models (e.g., Gray *et al* 2010). One hypothesis for how solar variability can affect weather and climate is that solar variability imposed on the interplanetary magnetic field (IMF) modulates the meteorological action of the global atmospheric electric circuit (GEC) in the polar regions. This IMF GEC hypothesis can be broken down into three parts. In summarising these here we emphasise which parts are supported by experimental evidence with a particular focus on Antarctica:

(i) Electric field and current anomaly. It is well established empirically and theoretically that variations in the IMF change the horizontal electric field in the polar ionosphere (e.g., Pettigrew *et al* 2010). For example, a change in the IMF from ~5 nT dawnward to ~5 nT duskward causes the ionospheric electric potential to increase by >20 kV everywhere within a latitudinal radius of ~15° of the southern geomagnetic pole (and similarly decrease the potential around the north geomagnetic pole) (Lam *et al* 2013). Theoretically, this should cause a corresponding change in the ionosphere-to-ground potential and hence vertical electric field throughout the atmospheric column (Lucas *et al* 2015). Since all levels of the atmosphere are ionized, by cosmic rays, solar radiation, and surface radioactive sources (Aplin and Harrison 2015), there will also be a corresponding anomaly in the vertical current. Both the vertical electric field and current anomalies have been isolated in measurements on the ground (Burns *et al* 2006, Panneersevam *et al* 2007) and in the stratosphere (Byrne *et al* 1991) in Antarctica.

(ii) Effect on cloud microphysics. Continuity of this vertical current through a stratiform cloud will cause electrical charging at the cloud-air interface because the conductivity in clouds is relatively low due to ion loss by attachment to droplets (Harrison *et al* 2015). This has been clearly demonstrated in balloon measurements through clouds (Nicoll and Harrison 2016). This study includes observations from Halley, Antarctica.
It is theorised that this charging can change the droplet size distribution within clouds by influencing collisions (e.g., Harrison *et al* 2015, Tinsley and Zhou 2015). As yet, there is no empirical evidence to support this and consequently this is the most uncertain link in the chain of processes in the GEC hypothesis (Lam *et al* 2014).

(iii) Meteorological response. If the droplet size distribution is changed in Antarctic clouds by mechanisms (i) and (ii) then this will alter radiative forcing (e.g., Lachlan-Cope 2010), causing large-scale Antarctic surface atmospheric pressure anomalies (e.g., Lubin *et al* 1998).

A model of the electric field and current anomaly (i) has been developed within an atmospheric GCM framework (Lucas *et al* 2015) but the meteorological response (iii) has yet to be included because our understanding of the cloud microphysics (ii) is still to be adequately developed.

However, consistent with the above GEC hypothesis, observations have shown that there are correlations between fluctuations in the daily mean of the duskward component, B_y, of the IMF and surface air pressure variations (Mansurov *et al* 1974, Page 1989, Tinsley and Heelis 1993, Burns *et al* 2007, 2008, Lam *et al* 2013, 2014). This correlation, often referred to as the Mansurov effect, is the clearest and most direct example of a meteorological response to changes in the GEC (Tinsley 2008, Lam and Tinsley 2015). Using data from 11 Antarctic and 7 Arctic stations over the interval 1995–2005, linear regressions of noontime surface air pressure on daily average IMF B_y yielded highly statistically significant correlations in the Antarctic over the entire interval 1995–2005, but in the Arctic over only the interval 1999–2002 (table 1 of Burns *et al* 2008). Regression coefficients corresponded to a change in pressure of ~1–2 hPa from a variation in B_y of ~8 nT. Using reanalysis data, differences in polar noontime surface air pressure of similar amplitude and significance were also found between samples during which daily average IMF $B_y > 3$ nT and $B_y < -3$ nT over the interval 1999–2002 (Lam *et al* 2013). In both studies the relationship between pressure and B_y is of opposite sign in the Arctic and Antarctic for 1999–2002, as expected from the GEC hypothesis (Burns *et al* 2008, Lam *et al* 2013). More recently, a hemispherically asymmetric relationship has also been reported between IMF B_y and zonally-averaged surface pressure above ~70° latitude in reanalysis data when averaged over 21 years (1995–2015) and over each of the two separate decades within this (1995–2005 and 2006–2015), which approximately correspond to the last two solar cycles 23 and 24 (Zhou *et al* 2018).

Extending the Lam *et al* (2013) analysis from the surface up into the stratosphere, a highly significant (99% field significance level) correlation was also found between IMF B_y and pressure throughout the Antarctic troposphere (Lam *et al* 2014). The varying time lag with height of the peak correlation provides evidence that the effect originates in the lower troposphere and propagates upwards to the tropopause, consistent with a cloud source.

In addition, there is observational and theoretical evidence that the Mansurov effect in both polar regions modifies the quasi-stationary planetary wave field at mid-latitudes (Lam *et al* 2013).

Quite recently, a temperature anomaly associated with IMF B_y has been found, of about 0.7 °C averaged over the region poleward of 70 °S and extending up to the 500 hPa atmospheric pressure level (Lam *et al* 2018). In this paper, we use a similar statistical method (section 2) to identify the sub-Antarctic extension of this temperature anomaly between ~65 °S and 50 °S at the surface, showing seasonal and inter-annual variations of its geographical structure (section 3.1). By exploiting particularly simple structural properties of the atmosphere existing in this region over the autumns of 1999–2002, we also elucidate some of the physics behind the sub-Antarctic surface temperature anomaly (section 3.2). In this case, we show that the anomaly can be modelled by meridional temperature advection by the geostrophic wind of the Mansurov pressure anomaly and that the amplitude of the temperature anomaly is controlled by the decorrelation time of IMF B_y. However, the assumptions used in the model are not expected to generally apply and so the model cannot describe the seasonal and inter-annual variability in the temperature anomaly structure. Overall, we conclude (section 4) that there is both statistical and physical evidence that the surface temperature anomaly is due to the Mansurov effect in which surface air pressure is influenced by IMF B_y, consistent with the IMF GEC hypothesis.

2. Data and methodology

We analyze the surface air temperature anomaly with the same method and data sources used to examine the surface air pressure anomaly (Lam *et al* 2013): We begin with surface air temperature data $T(\lambda, \varphi, y, m, d, h)$

from the National Centers for Environmental Prediction/National Center for Atmospheric Research (NCEP/NCAR) reanalysis dataset (Kalnay *et al* 1996). Geographic location is sampled at 2.5° intervals in latitude λ and longitude φ, and four time samples per day are defined here by year y, month m, day d, and hour h.

The climatological temperature variation T_c is then removed to yield an adjusted daily temperature $T_a(\lambda, \varphi, y, m, d) = T_{12} - T_c$. Here $T_{12} = T(\lambda, \varphi, y, m, d, h = 12)$ is the 12 UT surface temperature and $T_c = \langle T_{12} \rangle_Y$ is the average of this over the set Y of all available years for each day of year and at each location. The available years for this study were 1948 to 2011. Using a fixed $h = 12$ UT value effectively removes the diurnal variation, and averaging over all years keeping the other variables fixed approximates the seasonal cycle.

For a given set of dates S, such as the 1999–2002 time interval used in our original study (Lam *et al* 2013), we then identify the subset of dates S^+ when daily-mean IMF B_y is large and positive ($\geqslant$3 nT). To do this we use IMF data from the OMNI dataset (King and Papitashvili 2005) in the geocentric solar magnetospheric (GSM) coordinate system, where positive B_y is aligned from dawn to dusk. For the subset S^+, we calculate the mean of the adjusted temperature at each location $T^+(\lambda, \varphi) = \langle T_a(\lambda, \varphi, y, m, d) \rangle_{S^+}$. Similarly, we also calculate the mean of the adjusted temperature $T^-(\lambda, \varphi) = \langle T_a(\lambda, \varphi, y, m, d) \rangle_{S^-}$ for the subset of dates S^- in S when daily-mean IMF B_y is large and negative ($\leqslant -3$ nT). We define the difference in these two means as $\Delta T = T^+ - T^-$. The equivalent pressure quantity is $\Delta p = p^+ - p^-$. We will refer to ΔT and Δp as the IMF B_y-related air temperature and pressure anomalies.

To test the null hypothesis that there is no difference in the population of adjusted surface temperature values for IMF $B_y \geqslant 3$ nT compared with that for IMF $B_y \leqslant -3$ nT (and hence $T^+ = T^-$ and $\Delta T = 0$), we conduct a non-parametric Wilcoxon Rank-Sum test at each location. The test statistic Z is the standardized sum of the ranks of one sample, which is approximately normally distributed. The statistical significance of the result is then the one-tailed probability of obtaining a value of Z or greater by chance from the standard normal distribution. The result of this test is commonly referred to in one of two ways: for a one-tailed probability $P = 0.01$, we can say that the probability of obtaining a value greater than Z by chance is 1%, or we can say (as we do in this paper) that the null hypothesis can be rejected at the 99% confidence level. We also test the field significance of whether the positive and negative B_y samples of T_a are significantly different over a region. Following Wilks (2006), the field significance is well approximated simply by the minimum P value in the region.

In our previous studies (Lam *et al* 2013, 2014, 2018), the set S comprised all days in the interval 1999–2002. Here, we now separate our analysis into the four austral seasons: summer (December, January and February—DJF), autumn (March, April and May—MAM), winter (June, July and August—JJA), and spring (September, October and November—SON). We also briefly examine how the temperature anomaly evolves over contiguous four-year intervals in the interval 1995–2010. In the context of the IMF GEC hypothesis, this approximately corresponds to solar cycle 23. Shorter intervals are not considered as the sample sizes of the large positive and negative B_y sets S^+ and S^- become potentially too small to be statistically reliable, e.g., $<\sim$50 samples for individual years in 1995–1997 and 2004–2010.

In all cases, we analyze the region poleward of 50 °S. Within this lies the polar front between the Ferrel and polar cells of atmospheric circulation at ~60 °S. The 70 °S circle roughly divides the cold and orographically-complicated Antarctic continent from the relatively warm and flat Southern Ocean. Figure 1 shows a map of Antarctica and identifies some key regions that will be referred to below.

3. Results

3.1. Statistical identification of the IMF B_y-related surface air temperature anomaly and its inter-annual and seasonal variation

The IMF B_y-related surface air temperature anomaly field ΔT has considerable inter-annual variability over the interval 1995–2010. In figure 2, we show ΔT poleward of 50 °S averaged over successive 4-year intervals: (a) 1995–1998, which includes the solar minimum of solar cycle 22/23 and rising phase of the solar cycle 23, (b) 1999–2002, around solar maximum and early declining phase, (c) 2003–2006, late declining phase, and (d) 2007–2010, the prolonged solar minimum of solar cycle 23/24 (Hathaway 2015). In each interval, there is considerable spatial variation of ΔT with both negative and positive anomalies. The range of ΔT is of a similar size in all intervals but broadly highest in 2007–2010 (figure 2(d)) and lowest in 2003–2006 (figure 2(c)). There is little similarity in the spatial structure of ΔT between intervals, suggesting considerable inter-annual variability to complicate our understanding of the temperature anomaly. The only stable feature we can identify is the sub-Antarctic region equatorward of ~65 °S in intervals 1995–1998 and 1999–2002 (figures 2(a), (b)). Here areas of clearly positive ΔT (i.e., reddish) in one interval are typically also positive in that area in the other interval (or at least not clearly of the opposite sign, i.e., bluish). And conversely, for areas of clearly negative ΔT. Thus, we shall henceforth focus on the interval 1999–2002, which should minimize complications from inter-annual

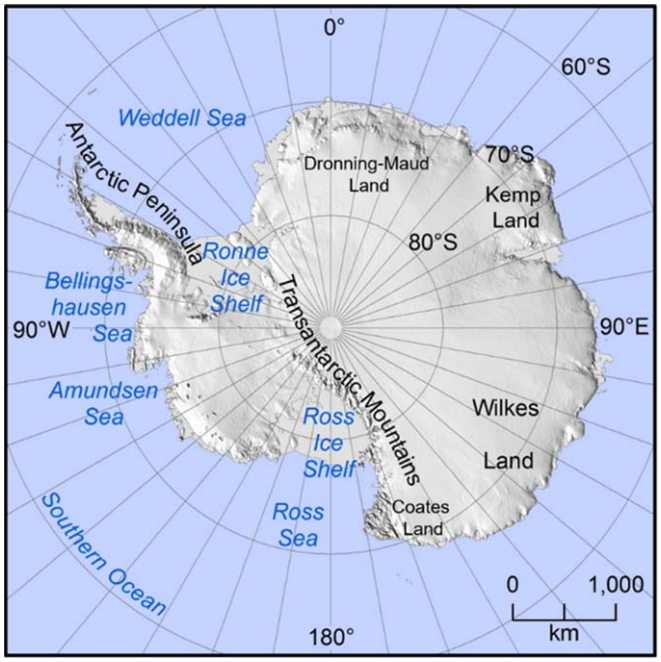

Figure 1. A map of Antarctica.

variability and take advantage of knowledge gained from our previous studies of this period (Lam *et al* 2013, 2014, 2018), as well as by Burns *et al* (2008).

The IMF *By*-related surface air temperature anomaly field ΔT over the interval 1999–2002 has a strong seasonal dependence (figure 3). To characterize this, we calculate a representative peak amplitude (RPA) of ΔT for each season over the region poleward of 60 °S where the largest anomalies lie. The RPA is defined as half the range between the 5th percentile of the ΔT distribution (which is always below 0°C) and the 95th percentile (always above 0 °C). The ΔT values at 5th and 95th percentiles are chosen rather than the peaks because they are more statistically stable. The largest RPA (3.2 °C) occurs in autumn (figure 3(b)), the next largest (2.4 °C) occurs in winter (figure 3(c)), with a slightly lower value in spring (figure 3(d)) of about 1.6 °C. The lowest RPA (0.9 °C) is in summer (figure 3(a)) when $|\Delta T|$ itself does not exceed 2°C anywhere in the Antarctic region.

It is thus evident that the mean $\Delta T \approx 0.7$ °C over Antarctica and over all seasons in 1999–2002 found by Lam *et al* (2018) belies considerable complexity in the spatial structure of ΔT and its variability. To understand some of the physics behind this, we will now focus on the autumn season in 1999–2002 (figure 3(b)), which has the largest amplitudes and levels of statistical significance for ΔT and, as we shall see later, is amenable to some theoretical analysis.

In this case, the spatial structure of ΔT can be characterized as follows: The largest positive values of ΔT are located in a region to the east of the Antarctic Peninsula—in the Weddell Sea and on the Ronne Ice Shelf (cf figure 1). Here there is a cluster of 20 grid points centered at 75.25°S, 314.25°E with each point value of $\Delta T \geqslant 5$ °C and above the 99.9% confidence level. Thus, the field significance of this region also exceeds the 99.9% confidence interval (Wilks 2006). The largest negative values occur in the Ross Sea and on the Ross Ice Shelf ($\Delta T \leqslant -6$ °C and above the 99.9% confidence level for a group of 31 grid points centered at 80°S, 195.65° E). Another significant area of positive ΔT occurs over and offshore of Wilkes Land ($\Delta T \geqslant 2$ °C and above the 99% confidence level for 25 grid points centered at 67.80°S, 114.20°E). More generally, equatorward of about the 70 °S circle that roughly defines the Antarctic coastline, the large-scale anomaly structure divides into three alternating positive and negative anomaly regions, each above the 90% confidence interval and with peaks above the 99% confidence interval. The three positive anomaly regions are in the Weddell and Ross sea sectors, and in the sector between Wilkes Land and Kemp Land. The three negative anomaly regions lie between these, in the Bellinghausen-Amundsen Sea, Coats Land, and Dronning-Maud Land sectors. Thus this suggests an $m \approx 3$ azimuthal wave structure over this entire 50–70 °S sub-Antarctic region with a field significance given by the lowest *P* value within the region (Wilks 2006), i.e., exceeding the 99% confidence interval.

3.2. Physical analysis of the surface air temperature anomaly

To investigate the physical origin of this spatial structure, figure 4(b) compares ΔT from figure 3(b) with the IMF B_y-related surface air pressure anomaly field Δp identified in our original study (Lam *et al* 2013). The zonal

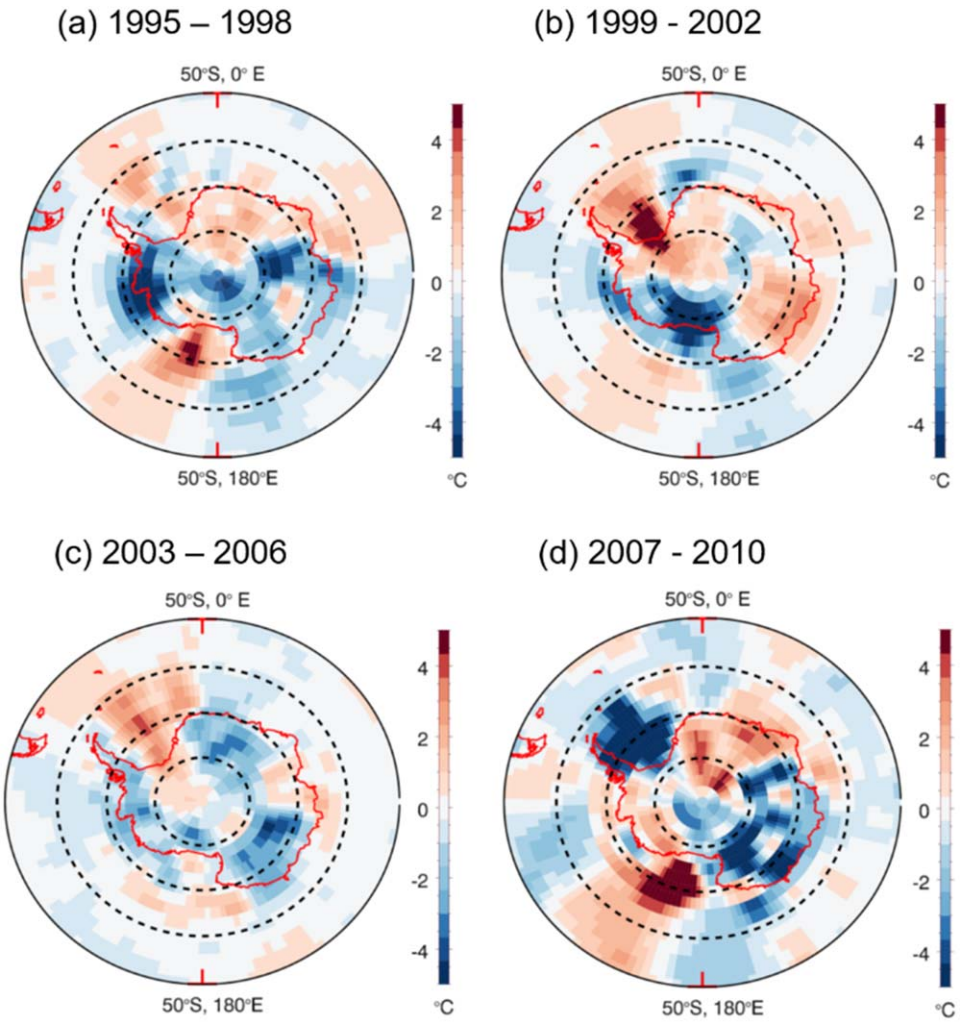

Figure 2. The IMF-B_y-related surface air temperature anomaly ΔT poleward of 50 °S in different 4-year intervals: (a) 1995–1998, (b) 1999–2002, (c) 2003–2006, and (d) 2007–2010. Dashed black circles mark 60, 70, and 80°S. The red contours bound Antarctica and other land masses.

structure of Δp equatorward of 70°S also resembles an $m \approx 3$ wave with anomaly lows (grey contours) centered near 40°E, 175°E, and 290 °E at 50 °S (the outer boundary of the figure). This $m \approx 3$ wave was first identified in the study of Lam *et al* (2013), but was not analyzed then according to season.

In the geostrophic approximation, where the forces due to friction and flow curvature are neglected such that the Coriolis and pressure gradient forces are balanced, air flows along isobars: clockwise around low pressure centres in the southern hemisphere. Thus the sub-Antarctic $m \approx 3$ wave in the surface air pressure anomaly creates a meridional wind anomaly such that air is perturbed poleward to the east of each of the three lows, and equatorward to the west of them. Now comparing also the Δp anomaly to the seasonal mean of the zonally-averaged surface air temperature T_z (figure 4(a)), there is a strong equatorward gradient in T_z such that a poleward wind anomaly can be expected to transport warm air towards Antarctica and an equatorward wind anomaly will transport cold air off Antarctica.

This then appears to explain the structure of ΔT in figure 4(b) in that the poleward wind anomalies (red boxes) carry warm air poleward to create positive ΔT anomalies and the equatorward wind anomalies (blue boxes) carry cold air equatorward to create negative ΔT anomalies. For example, in the Weddell Sea (~310°E), highly-meridional IMF B_y-related winds are, on average, drawing relatively warm air onto the Antarctic continent creating the $\Delta T \geqslant 5$ °C region remarked on earlier. On the other side of the Antarctic Peninsula, the IMF B_y-related wind draws air equatorward, off the continent, into the Bellingshausen and Amundsen Seas (~260°E) to create the $\Delta T \leqslant -2$ °C region. Elsewhere off the continent, the relationship between ΔT, meridional wind flow, and meridional gradient in zonal mean temperature also seems to hold. The only exception to the relationship is the area of negative ΔT centred at the coastal edge of the Ross Ice Shelf where our simple geostrophic analysis likely breaks down because the isobars of Δp are of high curvature.

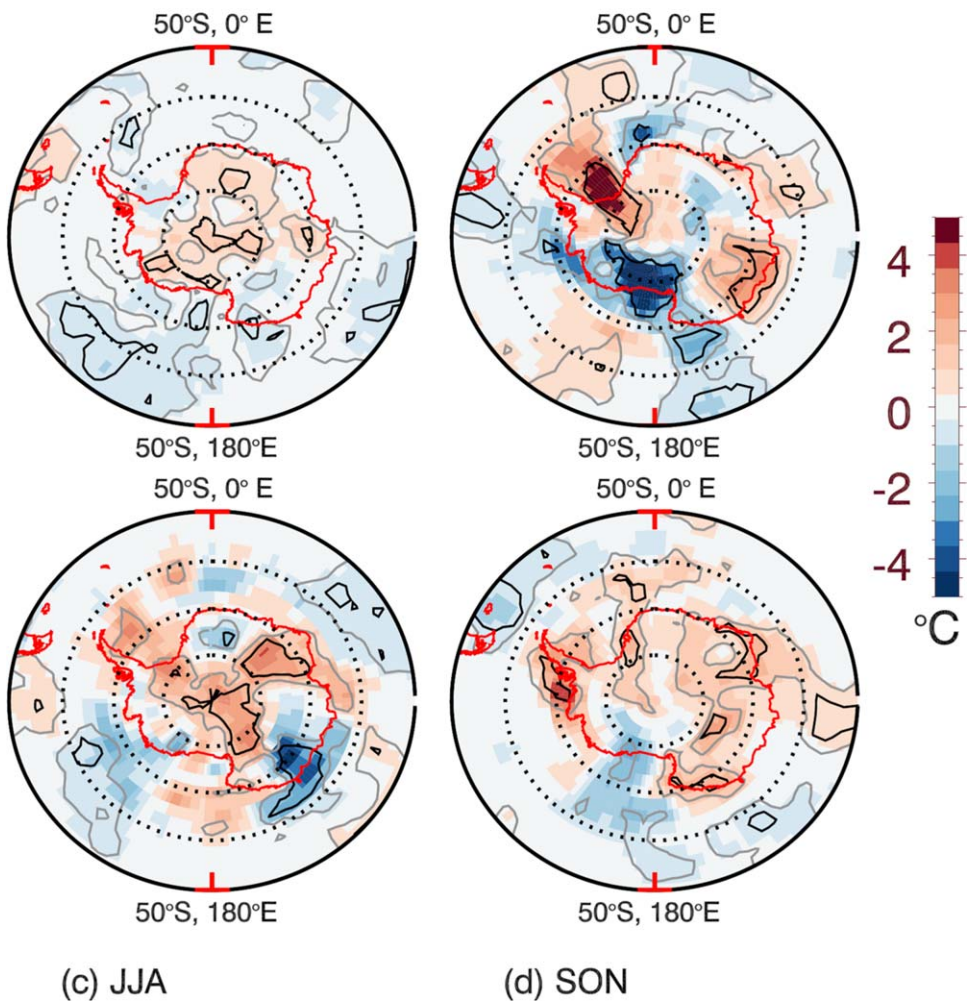

Figure 3. The IMF-B_y-related surface air temperature anomaly ΔT poleward of 50 °S in different seasons: (a) austral summer (DJF); (b) autumn (MAM); (c) winter (JJA); (d) spring (SON). Dotted black circles mark 60, 70, and 80°S. The red contours bound Antarctica and other land masses. Black and grey contours show statistical significance at the 99% and 90% levels, respectively.

To substantiate this, let us assume a model where the onset of a geostrophic wind anomaly due to an enhancement of IMF B_y at time $t = 0$ perturbs the motion of a parcel of air to advect it from some origin A to another location B, retaining the unperturbed (i.e., seasonal-average) temperature of its origin. If the seasonal-average temperature $\langle T \rangle$ is longitudinally invariant (as it approximately is—not shown) then the change in temperature at location B is given by the time integral of the meridional advective derivative of the unperturbed temperature due to the action of the perturbed flow $\mathbf{\Delta u}$ over the time τ taken to move from A to B:

$$\Delta T = -\int_0^\tau \frac{\Delta u_\theta}{r}\frac{\partial \langle T \rangle}{\partial \theta} dt \approx -\tau \frac{\Delta u_\theta}{r}\frac{\partial \langle T \rangle}{\partial \theta}$$
$$\approx \frac{\tau}{\langle \rho \rangle \Omega r^2 \sin 2\theta}\frac{\partial \Delta p}{\partial \varphi}\frac{\partial \langle T \rangle}{\partial \theta} \quad (1)$$

Here we use geographic spherical polar coordinates, where $r = 6371$ km is the Earth's radius, θ is co-latitude, and φ is longitude. The first approximation assumes that $\Delta u_\theta \tau$ is small compared to the length scale of variations in $\langle T \rangle$ and the second approximation is the geostrophic approximation, in which $\langle \rho \rangle$ is the atmospheric density and $\Omega = 7.29 \times 10^{-5}$ rad s^{-1} is the angular frequency of the Earth's rotation.

In figure 4(c) we show the model result ΔT using the timescale $\tau = 7$ h, seasonal averages $\langle \rho \rangle$ and $\langle T \rangle$ from the reanalysis dataset, and the pressure anomaly Δp calculated earlier and reproduced in figure 4(c). Comparing figures 4(c) to (b), it is clear that the model temperature anomaly is similar to the actual reanalysis temperature anomaly, suggesting the model is appropriate. (Note that for $\tau = 7$ h we find that $\Delta u_\theta \tau \sim 40$ km is indeed small, less than the 2.5° latitude resolution of the reanalysis dataset.)

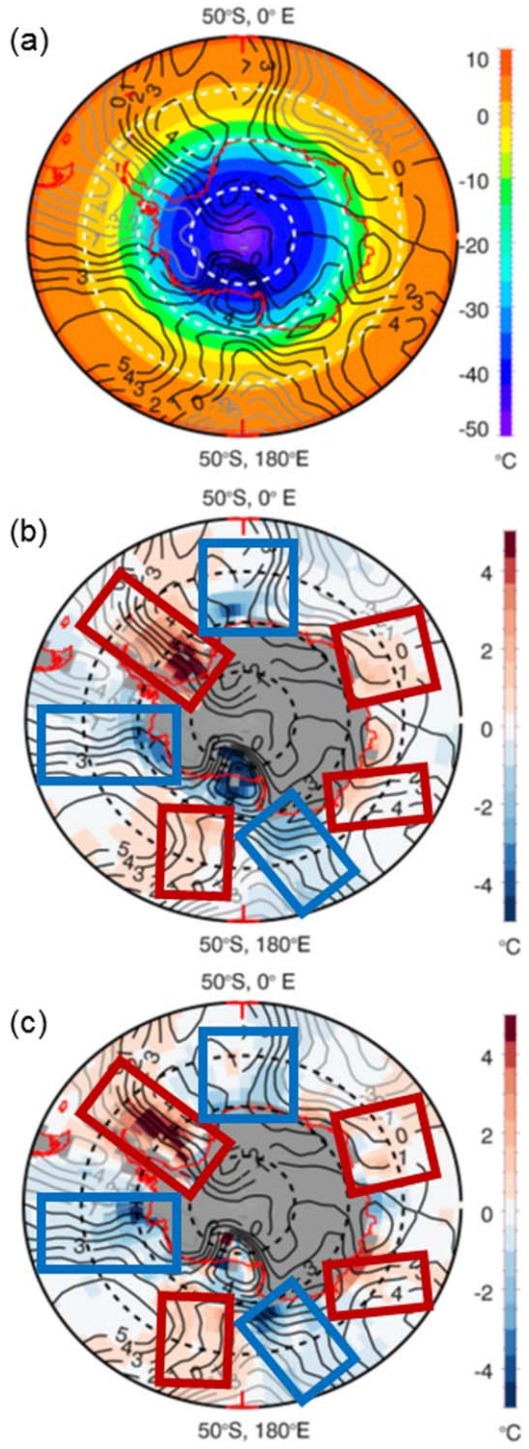

Figure 4. Relating the surface air temperature anomaly ΔT to the IMF-driven sea-level winds and the mean zonal mean air temperature in autumn. The pressure anomaly Δp, shown as contours poleward of 50 °S superimposed on: (a) The mean zonal mean air temperature T_z. (b) The anomaly ΔT. The grey area masks the region above sea level. Red boxes mark where the geostrophic wind flows poleward towards the Antarctic continent, and blue boxes mark flow equatorward away from the continent. (c) The ΔT anomaly estimated from equation (1). Dashed circles in each panel mark 60, 70 and 80 °S.

A possible interpretation of the timescale τ is that it is the time over which the anomalous geostrophic wind field persists. That is, according to our model, the temperature perturbation at location B will be the temperature of an isothermal parcel of air following a back-trajectory in a given perturbed geostrophic flow field. Assuming the IMF GEC hypothesis (see section 1), then that perturbed geostrophic flow field will be essentially fixed, as assumed in equation (1), for as long as IMF B_y remains in a given state, e.g., $B_y \geqslant 3$ nT. Longer than this, B_y will be different and hence the geostrophic flow field will be different. By this argument, we expect τ to be the decorrelation time of IMF B_y, i.e., the time for which B_y retains some memory of its previous state. Referring to figure 5, we find that the variation of B_y on short time scales (lag $L < 1$ day) can be approximated by an AR(1)

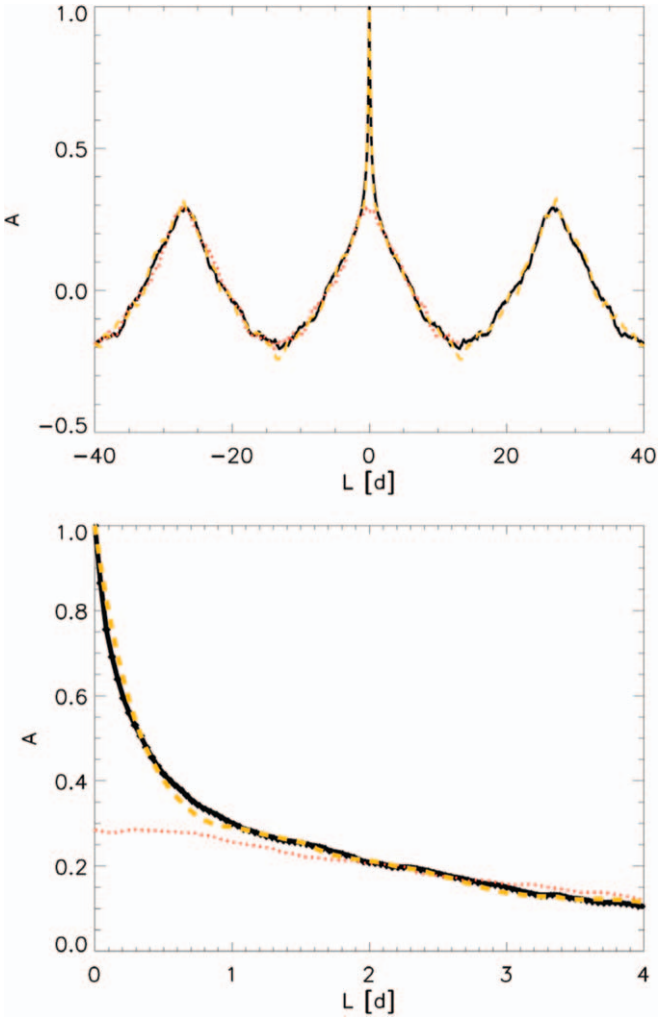

Figure 5. Autocorrelation function (ACF) of IMF B_y. Top panel: The black curve shows the ACF of 1-hour averaged IMF B_y from 1999–2002 for lags $-40 \leqslant L \leqslant 40$ days. The red dotted curve shows a replica of the ACF for lags $13 \leqslant L \leqslant 40$ days shifted by -27 and -54 days in order to demonstrate the periodic structure at the $\tau_{sc} = 27$ day solar rotation period. The orange dashed curve shows the ACF of a model of IMF B_y given by $B_y(t) = \mathrm{sgn}\,(2\pi t/\tau_{sc}) + a\ \ \mathrm{sgn}\,(2\pi t/\tau_{sc}) + bB_y(t-\delta) + \varepsilon$ where $a = 0.4,\ \ b = 0.87$, $\delta = 1$ h, and ε is a normally-distributed random variable with zero mean and standard deviation $\sigma = 0.8$. Bottom panel: An expanded version of the top panel for lags $0 \leqslant L \leqslant 4$ days.

process with a decorrelation time $\tau = 7$ h, exactly matching that used in equation (1) to produce the model temperature anomaly (figure 4(c)) that reproduces the empirical anomaly (figure 4(b)).

In summary, by close examination of the sub-Antarctic region in 1999–2002 austral autumn we deduce that the statistically-significant temperature anomaly ΔT associated with IMF B_y (figure 4(b)) is consistent with a model (figure 4(c)) in which the Mansurov surface pressure anomaly Δp associated with IMF B_y (figures 4(b), (c)) creates a geostrophic flow anomaly that isothermally transports the unperturbed air (figure 4(a)) for the time $\tau = 7$ h over which B_y persists in the state consistent with Δp (figure 5). Thus, our detailed analysis of this season provides some physical evidence in support of the IMF GEC hypothesis beyond relying on the statistical significance of the identified anomalies.

Applying the model given by equation (1) to the empirical sub-Antarctic temperature anomaly in the other seasons in the 1999–2002 interval (figure 3), we find (not shown) that the anomaly magnitude is reasonably well reproduced, broadly consistent with the changing latitudinal gradient of the seasonal-average temperature. However, its spatial structure is less well explained. This is not really surprising given the assumptions used to derive equation (1), which are unlikely to be generally satisfied from season to season, as well as from year to year (figure 2). For example, the simple $m \approx 3$ structure of Δp appears to break down in other seasons (not shown) which may weaken the geostrophic approximation, and the isothermal approximation is generally unexpected. This emphasises the need to improve our understanding of postulated interaction of the GEC with clouds such that the IMF GEC hypothesis may be implemented and tested in a general circulation model (see section 1) and its wider meteorological impacts explored.

Assuming our interpretation is correct, it is perhaps remarkable that the relatively feeble electromagnetic power input to the Earth system associated with the IMF (10^{13} W at most (Koskinen *et al* 2002) compared to the 10^{17} W of incoming solar radiation) is able to cause such large regional temperature anomalies. Clearly, the temperature response is highly non-linear. The effect of the IMF on atmospheric pressure is fairly weak. As can be seen in figure 4, the pressure perturbation is predominantly an $m \approx 3$ wave with an amplitude of about 4 hPa around the 60 °S latitude circle say. This corresponds to a geostrophic wind perturbation of about 1.6 m s^{-1}, corresponding to a light breeze on the Beaufort scale. However, its effect on temperature is greatly amplified by the wind carrying air across the strong background latitudinal temperature gradient, particularly in the autumn season studied in detail here. It is this role of the IMF GEC in regulating heat transport that appears to be main source of the observed non-linear response.

4. Conclusions

We have analyzed seasonal and geographical dependences of surface air temperature anomalies in the Antarctic region due to differences in the IMF B_y component of the interplanetary magnetic field. Regional anomalies up to ~5 °C are found in 4-year averages between 1995 and 2010 (approximately solar cycle 23) and in seasonal averages during 1999–2002. For the 1999–2002 interval, anomalies poleward of 60 °S have representative peak amplitudes in autumn, winter, spring and summer of 3.2 °C, 2.4 °C, 1.6 °C and 0.9 °C, respectively. In 1999–2002 autumn, the localized temperature anomalies to the east and the west of the Antarctic Peninsula were found to be 5 °C in the Weddell Sea and −2 °C in the Amundsen Sea and have a $m \approx 3$ wave structure in the sub-Antarctic region. We have demonstrated that the sub-Antarctic autumn temperature anomalies result from IMF B_y-driven changes to surface atmospheric pressure attributed to the global atmospheric electric circuit (Lam *et al* 2013, 2014) that drive air across the large meridional gradients in air temperature between 50 and 70°S, i.e., in the Southern Ocean outside Antarctica. Given the size of the temperature anomalies, we conclude that it is important to understand the mechanisms behind these global atmospheric electric circuit-related influences on meteorology, and to implement and test them in numerical models.

Acknowledgments

NCEP/NCAR reanalysis data were provided by the NOAA/OAR/ESRL PSD, Boulder, Colorado, USA, from their website www.esrl.noaa.gov/psd/. We acknowledge use of NASA/GSFC's Space Physics Data Facility's OMNIWeb service at http://omniweb.gsfc.nasa.gov. MML was supported to do this work by a Philip Leverhulme Prize (no associated grant number) won by Prof Mathew Owens (University of Reading). The authors also acknowledge support by UK Natural Environmental Research Council (NERC) grant NE/I024852/1 and also core funding from the NERC to the British Antarctic Survey's Space Weather and Atmosphere programme. We thank John Turner and Gareth Chisham from the British Antarctic Survey (BAS) for useful discussions, and the BAS Mapping and GIS team for the map.

ORCID iDs

Mervyn P Freeman https://orcid.org/0000-0002-8653-8279
Mai Mai Lam https://orcid.org/0000-0002-0274-6119

References

Aplin K L and Harrison R G 2015 Electricity in the atmosphere: Ions in the Atmosphere *Encyclopedia of Atmospheric Sciences* (3) 2nd edition (Amsterdam: Elsevier) 9–13978-0-12-382225-3

Burns G B, Tinsley B A, Klekociuk A R, Frank-Kamenetsky A V, Duldig M L, Bering E A and Clem J M 2006 Antarctic polar plateau vertical electric field variations across heliocentric current sheet crossings *J. Atmos. Sol. Terr. Phys.* **68** 639–54

Burns G B, Tinsley B A, Frank-Kamenetsky A V and Bering E A 2007 Interplanetary magnetic field and atmospheric electric circuit influences on ground-level pressure at Vostok *Journal of Geophysical Research: Atmospheres* **112** D04103

Burns G B, Tinsley B A, French W J R, Troshichev O A and Frank-Kamenetsky A V 2008 Atmospheric circuit influences on ground-level pressure in the Antarctic and Arctic *Journal of Geophysical Research: Atmospheres* **113** D15112

Byrne G J *et al* 1991 Balloon observations of stratospheric electricity above the South Pole : vertical electric field, conductivity, and conduction current *J. Atmos. Terr. Phys.* **53** 859–68

Gray L J *et al* 2010 Solar influence on climate *Rev. Geophys.* **48** RG4001

Harrison R G, Nicoll K A and Ambaum M H P 2015 On the microphysical effects of observed cloud edge charging *Q. J. R. Meteorolog. Soc.* **141** 2690–9

Kalnay E *et al* 1996 The NCEP/NCAR 40-year reanalysis project *Bull. Am. Meteorol. Soc.* **77** 437–71

King J H and Papitashvili N E 2005 Solar wind spatial scales in and comparisons of hourly Wind and ACE plasma and magnetic field data *Journal of Geophysical Research: Space Physics* **110** A02104

Koskinen H E J and Tanskanen E I 2002 Magnetospheric energy budget and the epsilon parameter *Journal of Geophysical Research: Space Physics* **107** (A11) 1415
Lachlan-Cope T 2010 Antarctic clouds *Polar Res.* **29** 150–8
Lam M M, Chisham G and Freeman M P 2013 The interplanetary magnetic field influences mid-latitude surface atmospheric pressure *Environ. Res. Lett.* **8** 045001
Lam M M, Chisham G and Freeman M P 2014 Solar wind-driven geopotential height anomalies originate in the Antarctic lower troposphere *Geophys. Res. Lett.* **41** 6509–14
Lam M M and Tinsley B A 2015 Solar wind-atmospheric electricity-cloud microphysics connections to weather and climate *J. Atmos. Sol. Terr. Phys.* **149** 277–90
Lam M M, Chisham G and Freeman M P 2018 IMF-driven change to the Antarctic tropospheric temperature due to the global atmospheric electric circuit *J. Atmos. Sol. Terr. Phys.* **180** 148–52
Lubin D, Chen B, Bromwich D H, Somerville R C J, Lee W-H and Hines K M 1998 The Impact of Antarctic Cloud Radiative Properties on a GCM Climate Simulation *J. Clim.* **11** 447–62
Lucas G M, Baumgaertner A J G and Thayer J P 2015 A global electric circuit model within a community climate model *Journal of Geophysical Research: Atmospheres* **120** 12054–66
Mansurov S M, Mansurova L G, Mansurov G S, Mikhnevich V V and Visotsky A M 1974 North-south asymmetry of geomagnetic and tropospheric events *J. Atmos. Sol. Terr. Phys.* **36** 1957–62
Nicoll K A and Harrison R G 2016 Stratiform cloud electrification: comparison of theory with multiple in-cloud measurements *Q. J. R. Meteorolog. Soc.* **142** 2679–91
Page D E 1989 The interplanetary magnetic field and sea level polar atmospheric pressure ed S K Avery and B A Tinsley *Workshop on Mechanisms for Tropospheric Effects of Solar Variability and the Quasi-Biennial Oscillation* p 227 (United States of America: University of Colorado, Boulder, Colorado)
Panneerselvam C, Selvaraj C, Jeeva K, Nair K U, Anilkumar C P and Gurubaran S 2007 Fairweather atmospheric electricity at Antarctica during local summer as observed from Indian station, Maitri *J. Earth Syst. Sci.* **116** 179–86
Pettigrew E D, Shepherd S G and Ruohoniemi J M 2010 Climatological patterns of high-latitude convection in the Northern and Southern hemispheres: Dipole tilt dependencies and interhemispheric comparisons *Journal of Geophysical Research: Space Physics* **115** A07305
Tinsley B A 2008 The global atmospheric electric circuit and its effects on cloud microphysics *Rep. Prog. Phys.* **71** 066801
Tinsley B A and Heelis R A 1993 Correlations of atmospheric dynamics with solar activity: Evidence for a connection via the solar wind, atmospheric electricity, and cloud microphysics *Journal of Geophysical Research: Atmospheres* **98** 10375–84
Tinsley B A and Zhou L 2015 Parameterization of aerosol scavenging due to atmospheric ionization *Journal of Geophysical Research: Atmospheres* **120** 8389–410
Wilks D S 2006 On 'field significance' and the false discovery rate *Journal of Applied Meteorology and Climatology* **45** 1181–89
Zhou L, Tinsley B A, Wang L and Burns G 2018 The zonal-mean and regional tropospheric pressure responses to changes in ionospheric potential *J. Atmos. Sol. Terr. Phys.* **171** 111–8